Optoelectronic properties of laser-beam-patterned few-layer lateral MoS$_2$ Schottky junctions

Y. Nagamine, J. Sato, Y. Qian (iD), T. Inoue (iD), T. Nakamura (iD), S. Maruyama (iD), S. Katsumoto (iD), and J. Haruyama (iD)

View Online   Export Citation   CrossMark

Optoelectronic properties of laser-beam-patterned few-layer lateral MoS$_2$ Schottky junctions

Y. Nagamine,[1] J. Sato,[1] Y. Qian,[2] (iD) T. Inoue,[2] (iD) T. Nakamura,[3] (iD) S. Maruyama,[2] (iD) S. Katsumoto,[3] (iD) and J. Haruyama[1,4,a] (iD)

AFFILIATIONS

[1]Faculty of Science and Engineering, Aoyama Gakuin University, 5-10-1 Fuchinobe, Sagamihara, Kanagawa 252-5258, Japan
[2]Department of Mechanical Engineering, The University of Tokyo, 7-3-1 Hongo, Bunkyo-ku, Tokyo 113-8656, Japan
[3]Institute for Solid State Physics, The University of Tokyo, 5-1-5 Kashiwanoha, Kashiwa, Chiba 277-8581, Japan
[4]Institute for Industrial Science, The University of Tokyo, 4-6-1 Komaba Meguro-ku, Tokyo 153-8505, Japan

[a]Author to whom correspondence should be addressed: J-haru@ee.aoyama.ac.jp

ABSTRACT

Atomically thin (or few-layer) two-dimensional transition metal dichalcogenide (TMDC) materials have various unique optoelectronic properties, which bring advantages for application to flexible solar cells and photodetectors, by bandgap engineering via van der Waals hybridization. TMDCs have crystal phase structures, such as the 2H semiconducting phase and the 1T (or 1T′) metallic phase. Recently, we demonstrated the creation of few-atom-layer 1T-metal/2H-semiconductor molybdenum disulphide (MoS$_2$) lateral Schottky junctions by using electron beam (EB) irradiation and revealed their unique optoelectronic properties. However, the 1T phase is metastable, whereas the 1T′ phase is more stable and useful for various applications. Here, we create a few-layer 1T′-metal phase MoS$_2$ by laser beam irradiation, which is a simpler, convenient, and low-cost method compared to EB irradiation. We observe unique optoelectronic features of the few-atom-layer 1T′-metal/2H-semiconductor lateral Schottky junctions in reverse bias voltage regions, such as an effective barrier height of ∼0.15 eV, highly efficient photogeneration ratios (>20%), and high sensitivity to photoirradiation angles without degradation for one month. These properties show great promise for application to highly efficient, flexible, and semitransparent photodetectors and solar cells with long-term reliability.

Flexible and (semi)transparent photodetectors and solar cells are attracting significant attention for various applications. From this perspective, atomically thin transition metal dichalcogenides (TMDCs) have high potential because of their unique semiconducting properties, semitransparent layers, and high mechanical flexibility. Optoelectronic properties have been reported in various atomically thin TMDCs (e.g., a MoS$_2$/WS$_2$ PN junction created by van der Waals assembly[1]). This PN junction revealed that the tunneling-assisted interlayer recombination of the majority carriers [i.e., Shockley–Read–Hall (SRH) recombination and Langevin recombination] at the junction due to the lack of an extended depletion region is responsible for the tunability of the electronic and optoelectronic processes. The rapid separation of photogenerated charge carriers (i.e., exciton dissociation) at the PN junction was also observed through photoluminescence (PL) and photocurrent mappings. This ultrafast charge transfer was also reported in atomically thin MoS$_2$/WS$_2$ heterostructures[2] and our few-atom-layer MoS$_2$ with the electron-beam (EB)-derived lateral Schottky junction (SJ),[3,4] showing promise for applications to highly effective photodetectors.

As solar cells, atomically thin TMDCs demonstrate strong light–matter interactions, which are one order higher than those of conventional semiconductors (e.g., GaAs and Si[5]) and, thus, are highly anticipated to show good performance for effective, semitransparent, and flexible solar cells. One way to employ TMDCs for solar cells is to form heterojunctions with other solar cell materials (e.g., Si and GaAs), which enhance power conversion efficiency (PCE).[6–8] The other is to apply sole TMDCs, which are used as the photosensitive layers. A high PCE of 14% was obtained for thick nontransparent TMDCs with PN junctions,[9,10] whereas the PCE of few-layer semitransparent TMDCs is low, e.g., ∼0.01% for a PN-junction WSe$_2$ monolayer[11,12] and ∼0.5% for a vertically assembled WSe$_2$/MoS$_2$ layer.[1,13]

In contrast, SJ-based solar cells show great promise for obtaining high PCE with large integration for industrial applications. However, solar cells based on atomically thin (or few-layer) TMDCs are rare[14,15] although unique optoelectronic properties have been found in the lateral SJ using the 1T metallic phase for photodetector applications.[3,4]

Typically, a TMDC has different phases, e.g., the 2H semiconducting phase and the 1T and 1T′ metallic phases (Fig. 1). The 1T or 1T′ phases can be easily created by various methods. We previously showed that the 1T metallic phase can be imprinted into few-layer 2H-semiconducting MoS$_2$ by EB irradiation.[3] The interface of the EB-irradiated and nonirradiated (i.e., 1T/2H phases) regions demonstrated the formation of a lateral SJ with a barrier height (ϕ_B) in the range of 0.13–0.18 eV. The interface revealed various unique optoelectronic features, such as high sensitivity of the effective ϕ_B to electrostatic charge doping [e.g., via back gate voltage (V_{bg})], near freedom from Fermi level (E_F) pinning, and quick dissociation of photogenerated excitons due to the high concentration of electric fields. These led to effective photodetector performance.

However, EB irradiation carries high cost and requires a long time. Moreover, the 1T phase is metastable. In contrast, the 1T′ phase is more thermally and chemically stable, owing to the introduction of strain by decreasing the distance between two S atoms along the z direction (Fig. 1), which enables applications with long-term reliability. 1T′-TMDCs have been formed by various methods [e.g., laser beam

(LB) irradiation,[16–18] substrate heating,[19] and chemical vapor deposition on bi-layer graphene[20]] and deployed in various applications (e.g., Ohmic metallic junction between a metal electrode and 2H-MoS$_2$,[18] supercapacitor electrodes, and even as topological insulators[16,17,19,20]).

Here, we create a 1T′-metallic phase by applying LB irradiation to a 2H semiconducting phase and subsequently a 1T′/2H-semiconducting lateral SJ and reveal its unique optoelectronic behaviors. LB irradiation is a simpler, more convenient, and lower-cost method, compared to EB irradiation. This is a suitable process for industrial applications of highly efficient, flexible, and semitransparent photodetectors and solar cells.

In the present study, 2H-phase n-type semiconducting MoS$_2$ flakes were fabricated on an SiO$_2$/Si substrate following a mechanical exfoliation method of the bulk material (Smart material Co.) using scotch tape and oxidization by exposure to air [Fig. 1(b)]. The thickness (~3 nm) and number of layers (~five layers) were confirmed by cross-sectional atomic force microscopy, as shown in Fig. 1(c), and also by Raman spectroscopy [Fig. 1(i)]. A LB with a wavelength of ~532 nm, a diameter of ~1 μm, a power of ~4 mW, and a time of ~10 s per point was irradiated to the MoS$_2$ flake and scanned with a 0.1–0.2 μm overlapping region over an area of ~10 × 5 μm^2 at room temperature [as indicated by the red dotted rectangle in Fig. 1(e)].[11] This condition was employed based on our previous experiments for the quantum spin Hall effect,[16,17] which gave the smallest number of defects. LB-generated heat is accumulated over the regions scanned by the LB and the temperature of the regions reaches ~300 °C, resulting in a phase transition from 2H to 1T′ starting from the top surface layer [Fig. 1(f)]. Because excess heat accumulates from the top-surface side, such layers burn out and the layers become thinner [with a reduction of ~2 nm, as shown in Fig. 1(d)], resulting in a change to a (semi)-transparent appearance [Fig. 1(e)]. Remained bottom-side 1T′ metallic layers form a lateral 2H/1T′ SJ [Fig. 1(f)].

The presence of the 1T′ metallic phase has been confirmed by photoluminescence (PL) mapping, which indicates almost no signals with good uniformity [Fig. 1(g)], source–drain current vs voltage (I$_{sd}$–V$_{sd}$) features measured at three different points of the large 1T′ region sample [Fig. 1(h)], and Raman spectroscopy [peaks J$_1$–J$_3$ in Fig. 1(i)].[3] High uniformity of the 1T′ area is consistent between Figs. 1(g) and 1(h). Figure 1(h) shows the total resistance of ~14 KΩ and the contact resistance of ~200 Ω. Two electrodes [indicated by A and B in Fig. 1(e)] consisting of Ti/Au (20 nm/500 nm), one of which is located in the 1T′-metal region (i.e., LB-irradiated region), while the other is in the 2H region, were formed on both sides of the junction for photocurrent measurements. Ti/Au was selected in order to obtain a lower contact resistance to the n-type MoS$_2$ layer.[3] A back-gate electrode was also attached on the backside of the Si substrate with a thick SiO$_2$ layer (~300 nm). The measurements of photogenerated current (I$_{photo}$) were carried out using a solar cell simulator under standard test cell conditions (AM1.5G) at room temperature, using electrodes A and B shown in Fig. 1(e).

Figure 2(a) shows I$_{sd}$ at V$_{bg}$ = 0 V under dark and light ambient conditions for a sample after LB irradiation to cause the 1T′ transition. Weakly asymmetric I–V features were observed in the dark, and the asymmetry became much more significant for the reverse-V$_{sd}$ regions under light ambient conditions (i.e., with onset V$_{sd}$ of ~−0.6 V for the reverse current increase). This rectification property is much obvious in the inset of Fig. 2(a) for the wider V$_{sd}$ region. The current increase
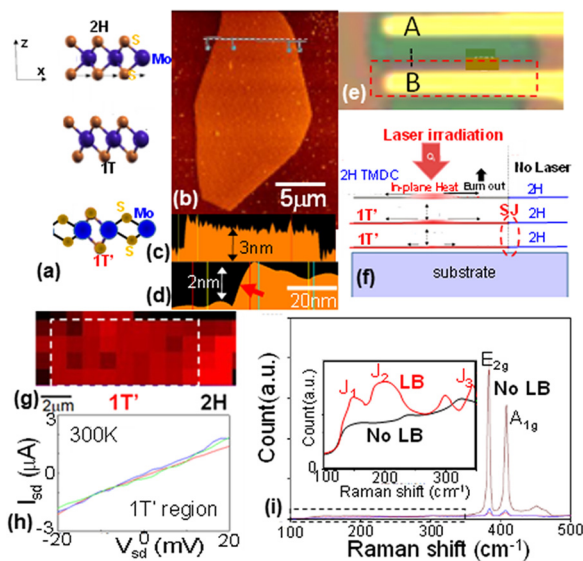

FIG. 1. (a) Schematic images of the crystal structure for 2H, 1T, and 1T′ phases. (b) and (c) Atomic force microscope (AFM) images of top (b) and cross-sectional (c) views of a few-layer 2H-MoS$_2$ flake fabricated by mechanical exfoliation of bulk material. (c) was measured along the white dotted line indicated in (b). (d) AFM cross-sectional view around the boundary for LB irradiated and nonirradiated regions shown by a short black dotted line in (e). A thick red arrow is the side surface with a gradual shape. (e) Optical microscope image of a part of (b) after LB irradiation. The irradiated regions become semitransparent owing to the low thickness. Two electrodes (A and B) are used for the electrical measurements. (f) Schematic view for LB irradiation to 2H semiconducting TMDC layers and formation of the 1T′ layers and the 2H/1T′ SJ. (g) PL mapping of the LB-irradiated 1T′ metallic region (surrounded by the white dotted-line) and nonirradiated 2H semiconducting region. The measured wavelength is between 640 and 700 nm, and the size of each rectangle is 1 μm^2. Darker regions have lower PL intensity. Those of the 1T′ area and the 2H area are less than 100 and larger than 3000, respectively. (h) I$_{sd}$–V$_{sd}$ curves measured at three different positions of the large 1T′ area sample. (i) Raman spectra of LB-irradiated and nonirradiated regions in (e). Inset: expansion of the main panel for the 100–350 cm^{-1} region (shown by the dotted rectangle).
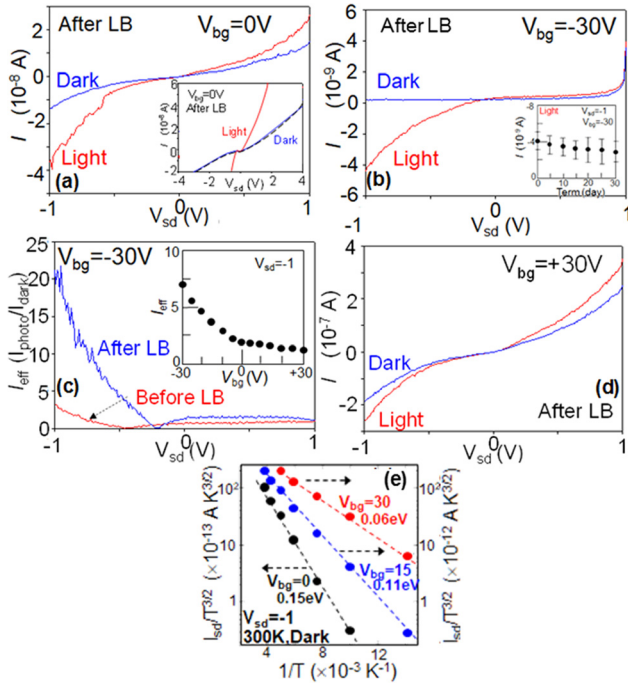
FIG. 2. (a), (b), and (d) Source–drain current (I_{sd}) measured between electrodes A and B in Fig. 1(g) for different V_{bg} values under dark and light ambient conditions. A solar cell simulator with standard test cell conditions (AM1.5G) was used at room temperature. Inset of (a): wider V_{sd} range of the main panel. The dotted curve is fit by 2D Schottky model. Inset of (b): currents of five samples with the Schottky junction (error bars) measured each 5 days for 30 days under light. (c) Generation efficiency (I_{eff}) of photocurrent (I_{photo}), that is, I_{photo} normalized by dark currents at $V_{bg} = -30$ V before and after the formation of the Schottky junction (i.e., LB irradiation). Inset: I_{eff} on V_{bg} at $V_{sd} = -1$ V. (e) Temperature dependence of I_{sd} on three different V_{bg} values at $V_{sd} = -1$ V under dark, as shown in the formalisms for the reverse voltage region of the 2D Schottky model [Eqs. (1)–(3)].

where A^*_{2D} is the 2D Richardson constant, W is the junction length ($\sim 10\,\mu m$), ϕ_B is the Schottky barrier height, k_B is the Boltzmann constant, m^* is the effective mass of MoS$_2$, and m_0 is the electron mass. All the dependences show linear relationships with ϕ_B ~ 0.15, ~ 0.11, and ~ 0.06 eV for V_{bg} values of 0, 15, and 30 V, respectively.

The result in Fig. 2(a) suggests the presence of a breakdown current, which originates from the concentration of high electric fields at the lateral SJ formed at the 2H/1T′ phase interface [see Fig. 4(a)] and supports the fact that the LB irradiation to the 2H semiconducting phase caused a transition to the 1T′ metallic phase, as confirmed by Raman observation. Figure 2(b) supports this because the n-type 2H-semiconducting region is almost electron-depleted by applying $-V_{bg}$. From this viewpoint, it is found that the result in Fig. 2(c) strongly supports the formation of the SJ by LB irradiation and represents a pure I_{photo} arising only from the large electric fields caused at the few-atom-layer 2H/1T′-phase lateral SJ [Fig. 4(b)]. This implies the extremely high efficiency of I_{photo} as a photodetector in the present SJ in the reverse voltage region (i.e., in $-V_{sd}$). Because electrons are heavily doped into the n-type 2H-semiconducting region by applying $+V_{bg}$ in Fig. 2(d) and the doped electrons significantly contribute to the detected currents [Fig. 4(c)], the current increase in $-V_{sd}$ disappears. The inset of Fig. 2(c) supports this argument. The temperature dependence of the dark current in Fig. 2(e) suggests the formation of a conventional 2D Schottky barrier in the present samples, as discussed later.

The dependence of I_{photo} on the photoirradiation angle θ of the sample with the Schottky junction (i.e., after LB irradiation) is shown in Figs. 3(a) and 3(b). θ is defined as the angle between the direction of photoirradiation and the sample surface [see the inset of Fig. 3(a)]. Thus, $\theta = 90°$ means a right angle, which gives the strongest photoirradiation magnitude to the sample surface. I_{photo} drastically increases
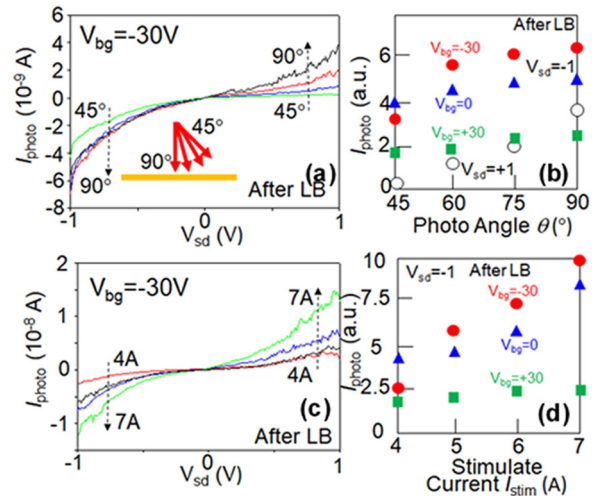
in the $-V_{sd}$ region became more evident under light at $V_{bg} = -30$ V, as shown in Fig. 2(b) (i.e., with an onset V_{sd} of ~ 0 V). I_{photo} normalized by dark current (I_{eff}) at $V_{bg} = -30$ V is demonstrated for the samples before and after LB irradiation in Fig. 2(c). After LB irradiation, I_{eff} drastically increases ($\sim$sevenfold) compared to I_{eff} measured before LB irradiation. When $+V_{bg}$ is applied, this feature disappears [Fig. 2(d)]; I_{eff} with respect to changing V_{bg}, which quantitatively demonstrates these features, is shown in the inset of Fig. 2(c). It clearly reveals a drastic decrease in I_{eff} with a change from $-V_{bg}$ to $+V_{bg}$. Short-circuit I_{photo} at $V_{sd} = 0$ V for solar cells is not observed in any cases.

The temperature dependence of I_{sd} on three different V_{bg} values under dark conditions is shown in Fig. 2(e), following the formalisms for the reverse voltage region of a two-dimensional (2D) Schottky model [Eqs. (1)–(3)],[3]

$$I_{2D} = WA^*_{2D}T^{3/2} \exp\left(\frac{q\phi_B}{k_B T}\right), \qquad (1)$$

$$A^*_{2D} = q\sqrt{8\pi k_B^2 m^*/h^2}, \qquad (2)$$

$$m^* = 0.45 m_0, \qquad (3)$$

FIG. 3. (a) Dependence of I_{photo} on photoirradiation angle θ of the sample with the Schottky junction at $V_{bg} = -30$ V. θ is defined as the angle between the direction of photoirradiation and the sample surface (inset). (b) I_{photo} (at $V_{sd} = -1$ V) vs θ for three different V_{bg} values (three colored-symbols) and that at $V_{sd} = +1$ V for $V_{bg} = -30$ V (empty circle). (c) Dependence of I_{photo} on the stimulated current (I_{stim}) to produce I_{photo} in the solar cell simulator at $V_{bg} = -30$ V. (d) I_{photo} (at $V_{sd} = -1$ V) vs I_{stim} for three different V_{bg} values.

as θ increases from 45° to 60° (by approximately a factor of two) and maintains the largest value at larger angles up to $\theta = 90°$ in the $-V_{sd}$ region of Fig. 3(a). In contrast, the increase in I_{photo} is gradual in the $+V_{sd}$ region, owing to the carrier increase in the 2H semiconducting region. This high sensitivity in the $-V_{sd}$ region becomes much weaker at $V_{bg} = 0$ and $+30$ V, where no electric fields concentrate on the SJ. This change is evident in Fig. 3(b). This result suggests that the few-layer lateral SJ with the high electric concentration at $-V_{sd}$ can act as a highly effective photodetector as θ increases. In another respect, I_{photo} remains nearly constant over a wide θ range (i.e., $60° \leq \theta \leq 90°$) with decreasing θ. This strongly implies that the present few-layer lateral SJ could provide a great advantage as a solar cell because I_{photo} could maintain the largest value (i.e., nearly that at $\theta = 90°$) even upon decreasing θ to 30°.

The dependence of I_{photo} on the stimulated current (I_{stim}) to produce I_{photo} in the solar cell simulator is demonstrated in Figs. 3(c) and 3(d). The increase in I_{photo} is drastic as I_{stim} changes from 4 to 7 A (by five times) at $V_{bg} = -30$ V for all V_{sd} regions [Fig. 3(c)]. This change decreases at $V_{bg} = 0$ and $= +30$ V. These sensitivities are shown in Fig. 3(d). This result also supports the highly efficient photocurrent generation of the present SJ in the reverse voltage region.

We now discuss the observed results. All the results suggest that large I_{photo} and I_{eff} can be produced by the concentration of high electric fields at the 2H/1T′ lateral SJ caused by applying reverse bias voltages, and the SJ acts as a highly effective photodetector. As we reported previously, the few-atom-layer 2H/1T lateral SJ formed by EB irradiation had unique properties.[20] In the present case, the 1T′ phase region is formed by heat accumulation (e.g., ∼300 °C) due to LB irradiation, and thus, the 1D SJ interface may not be sharp owing to thermal fluctuation. Indeed, the side surfaces of the burned-out area [indicated by a red arrow in Fig. 1(f)] are not sharp and are rather gradual. Nevertheless, we could confirm the formation of the conventional Schottky barrier as shown in Fig. 2(e). The estimated ϕ_B values are almost equal to those found in the EB-derived SJ at high temperatures ($\phi_B \sim 0.13$ eV). As shown in Fig. 4(c), increasing V_{bg} enhances electron doping into the 2H semiconducting region from the back-gate electrode and shifts E_F to a higher energy level. This reduces the E_F difference between the 1T′ and 2H regions, resulting in a decrease in effective ϕ_B. In the EB-derived SJ, the effective ϕ_B became zero [i.e., temperature-independent flat currents in Fig. 2(e)] at high temperatures in the large $+V_{bg}$ region. This resulted in a pinning-free E_F, despite the presence of interface defects in small amount. In the present case, such zero ϕ_B is not confirmed in Fig. 2(e). This may be attributed to the presence of a larger concentration of defects. Indeed, the onset of forward-voltage current is more gradual than those in the EB-derived

case and the estimated ideality factor $\eta \sim 1.2$ (meaning the generation/recombination currents by defects at the junction) is larger than that in the EB-derived case ($\eta \sim 1.07$), when the forward-voltage current is fit by the following formalism of the 2D SJ [inset of Fig. 2(a)].

The heat accumulation to cause the 1T′ phase may yield such a large concentration of defect centers, compared to the EB-derived case. However, we could efficiently detect I_{photo} and a large I_{eff} as well as the effective ϕ_B as mentioned above. This implies the usefulness of the present few-atom-layer lateral SJ, in which the concentration of high electric fields at $-V_{sd}$ causes the rapid dissociation of photogenerated excitons and the direct injection into (1T′) metal electrodes [Fig. 4(a)]. The observed optoelectronic features of five devices were maintained for one month at least [inset of Fig. 2(b)]. This is one of the advantages for the present few-layer structure. Oxidation is significant only at the topmost surface layer, and the inner layers below it are protected from oxidation by the surface layer. This promises long-term reliability of the present device as a high-efficiency photodetector.

Short-circuit I_{photo} is not confirmed in any of the present cases because the Schottky interface is a 1D line of only $\sim 10\,\mu m$ length. The improvement of the crystal quality of the Schottky interface and using longer total lines will be indispensable for obtaining short-circuit I_{photo} to realize high-efficiency solar cells. The observed photoresponse promises applications to high-efficiency photodetectors and possible solar cells, as well as to atomically thin optoelectronic circuits.

DATA AVAILABILITY

The data that support the findings of this study are available within this article.
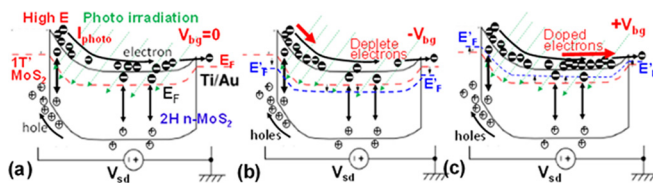

FIG. 4. Schematic views of energy band diagrams of the SJ for reverse voltage regions at (a) $V_{bg} = 0$ V, (b) $-V_{bg}$, and (c) $+V_{bg}$, which demonstrate that the high electric field concentrating at the atomically thin SJ causes effective exciton generation and its rapid dissociation, resulting in efficient photosensitivity.

REFERENCES

[1] C.-H. Lee, G. H. Lee, A. M. V. D. Zande, W. Chen, Y. Li, M. Han, X. Cui, G. Arefe, C. Nuckolls, T. F. Heinz, J. Guo et al., Nat. Nanotechnol. **9**, 676 (2014).

[2] X. Hong, J. Kim, S. F. Shi, Y. Zhang, C. Jin, Y. Sun, S. Tongay, J. Wu, Y. Zhang, and F. Wang, Nat. Nanotechnol. **9**, 682 (2014).

[3] Y. Katagiri, T. Nakamura, A. Ishi, C. Ohata, M. Hasegawa, S. Katsumoto, G. Iannaccone, G. Fiori, S. Roche, and J. Haruyama, Nano Lett. **16**, 3788 (2016).

[4] Y. Katagiri, T. Nakamura, S. Katsumoto, and J. Haruyama, Appl. Phys. Lett. **110**, 143109 (2017).

[5] M. Bernardi, M. Palummo, and J. C. Grossman, Nano Lett. **13**, 3664 (2013).

[6] O. L. Sanchez, E. A. Llado, V. Koman, A. F. i Morral, A. Radenovic, and A. Kis, ACS Nano **8**, 3042 (2014).

[7] M.-L. Tsai, S.-H. Su, J.-K. Chang, D.-S. Tsai, C.-H. Chen, C.-I. Wu, L.-J. Li, L.-J. Chen, and J.-H. He, ACS Nano **8**, 8317 (2014).

[8] S. Lin, X. Li, P. Wang, Z. Xu, S. Zhang, H. Zhong, Z. Wu, W. Xu, and H. Chen, Sci. Rep. **5**, 15103 (2015).

[9] S. Memaran, N. R. Pradhan, Z. Lu, D. Rhodes, J. Ludwig, Q. Zhou, O. Ogunsolu, P. M. Ajayan, D. Smirnov, A. I. Fernández-Domínguez et al., Nano Lett. **15**, 7532 (2015).

[10] S. Wi, H. Kim, M. Chen, H. Nam, L. J. Guo, E. Meyhofer, and X. Liang, ACS Nano **8**, 5270 (2014).

[11] D. J. Groenendijk, M. Buscema, G. A. Steele, S. M. de Vasconcellos, R. Bratschitsch, H. S. J. van der Zant, and A. Castellanos-Gomez, Nano Lett. **14**, 5846 (2014).

[12] B. W. H. Baugher, H. O. H. Churchill, Y. Yang, and P. Jarillo-Herrero, Nat. Nanotechnol. **9**, 262 (2014).

[13]R. Cheng, D. Li, H. Zhou, C. Wang, A. Yin, S. Jiang, Y. Liu, Y. Chen, Y. Huang, and X. Duan, Nano Lett. **14**, 5590 (2014).

[14]M. Fontana, T. Deppe, A. K. Boyd, M. Rinzan, A. Y. Liu, M. Paranjape, and P. Barbara, Sci. Rep. **3**, 1634 (2013).

[15]T. Akama, W. Okita, R. Nagai, C. Li, T. Kaneko, and T. Kato, Sci. Rep. **7**, 11967 (2017).

[16]H. Mine, T. Nakamura, T. Inoue, S. Pakdel, E. Z. Marin, S. Maruyama, S. Katsumoto, A. Fortunelli, J. J. Palacios, J. Haruyama et al., Phys. Rev. Lett. **123**, 146803 (2019).

[17]N. Katsuragawa, T. Nakamura, T. Inoue, S. Pakdel, S. Maruyama, S. Katsumoto, J. J. Palacios, and J. Haruyama, "Room-temperature quantum spin Hall phase in laser-patterned few-layer 1T′-MoS$_2$," Commun. Mater. (in press).

[18]S. Cho, S. Kim, J. Ho Kim, J. Zhao, J. Seok, D. H. Keum, J. Baik, D.-H. Choe, K. J. Chang, K. Suenaga et al., Science **349**, 625 (2015).

[19]S. Tang, C. Zhang, D. Wong, Z. Pedramrazi, H.-Z. Tsai, C. Jia, B. Moritz, M. Claassen, H. Ryu, S. Kahn et al., Nat. Phys. **13**, 683 (2017).

[20]Such pinning-free E_F and rapid dissociation of photogenerated excitons due to the concentration of high electric fields strongly contribute to the generation of a large I_{photo} because electrons and holes dissociate from the excitons rapidly, directly flow into individual electrodes, and are detected as I_{photo} [Fig. 4(b)]. As mentioned in the introduction, rapid exciton dissociation has been reported by observing the lack of the PL signal in an atomically thin P-WS$_2$/N-MoS$_2$ vertical junction. The interface is a 2D plane, whereas the lateral interface is a one-dimensional (1D) line. Thus, this effect is significantly enhanced in the lateral SJ, leading to applications as effective photodetectors.